

# A High Precision Time Measurement Method Based on Phase-Fitting for Muon Detection

Jianjun Wang, Zhao Wang, Jincheng Xu, Zhaohui Bu, Liguozhou, Qibin Zheng

**Abstract**—In order to simplify the muon detection system, this paper proposes a high-precision time measurement method based on phase-fitting by using the digitized muon pulses which are often used to extract the energy information of muons. Thus, the time and energy measurement can share a set of ADC modules, eliminating the need for separate hardware for time measurement. The relative time of flight (TOF) of muon pulses can be obtained with high precision through cross-correlation and phase fitting techniques. In this paper, the theory of time measurement based on this digital phase-fitting method was analyzed and an electronics prototype was designed to validate the feasibility of the method by utilizing a 40 MSPS ADC for muon pulse digitization and an FPGA for phase fitting implementation. The test results indicate that a time precision better than 50 ps was achieved when the signal-to-noise ratio (SNR) of the input pulse exceeds 64 dB. Furthermore, in cosmic ray tests, the prototype exhibited favorable timing performance. These results indicate that this proposed method has the potential to be a high-precision TOF measurement for muon and other nuclear pulse signals.

**Index Terms**—muon detection, phase fitting, time measurement, nuclear pulse detection

## I. INTRODUCTION

Muons are high-energy charged particles found in nature [1], characterized by their strong penetration ability, and they constitute an important component of cosmic rays [2]. The detection of muons demonstrates significant academic value across various fields, including particle physics [3], materials science [4], archaeology [5], and geology [6]. As scientific research progresses, the scale and precision requirements of muon detection experiments continue to grow. Large projects, represented by China's Circular Electron-Positron Collider (CEPC), are driving the pursuit of higher precision and larger-scale muon detection to meet the demands of exploring fundamental physical phenomena, thereby assisting scientists in identifying new particles such as the Higgs boson [7-10]. Additionally, the application of muon tomography in fields like archaeology and geology places increased demands on the resolution of detection systems [11, 12]. The expansion of

experimental scales with high resolution requirement has resulted in a significant increase in the number of readout electronic channels. Researchers have consistently focused on simplifying systems, increasing integration levels, and reducing power consumption.

The integration of time-to-digital converters (TDCs) with analog-to-digital converters (ADCs) in circuit boards designs [13-17] or chip-level integrations [18-21], has become the prevalent approach in muon detection systems. In these prevalent approaches, the ADC circuits are dedicated to measuring the muon energy information, while TDC technology is specifically employed for measuring the TOF information. Even though, advancements in TDC technology have contributed to a degree of improvement in the integration [22-26]. As the scale of multi-channel muon detection systems continues to expand, the application of independent circuits for energy and time measurements not only increases resource consumption of the system but also leads to higher costs. Therefore, it is essential to explore new, simple, and efficient measurement methods that can be implemented on circuit boards or Application-Specific Integrated Circuits (ASICs). Research has indicated that the digitized waveforms from ADC contain time information of the pulse signals, and this information can be estimated through correlation operations and spectral analysis based on waveform similarity [27, 28]. Muon pulse signals generally exhibit similar waveforms. Thus, an attractive solution is to perform time measurement of the muon digital waveforms through cross-correlation and spectral analysis. Effectively utilizing the time information within the digitized waveforms could facilitate higher integration and lower power consumption in large-scale muon detection systems.

This study proposes a time measurement method based on phase-fitting. Firstly, the muon signals are digitized by ADCs. Subsequently, while performing energy analysis within the FPGA, this method applies cross-correlation and phase fitting on the digital waveforms to calculate the time information. Distinct from the conventional time-domain techniques for time-delay estimation, this method estimates the time

Manuscript received xxx xx, 2024; revised xxx xx, xxx2024. This project is supported in part by grants from National Natural Science Foundation of China (No. 12105177 and 11904423) and a grant from National Key R&D Program of China (No. 2023YFF0719200), and support also from Shanghai Key Laboratory of Particle Physics and Cosmology (No. 22DZ2229013-1). (Corresponding author: Qibin Zheng;)

Jianjun Wang, Jincheng Xu, Zhaohui Bu, Liguozhou and Qibin Zheng are with the Quantum Medical Sensing Laboratory and School of Health Science and Engineering, University of Shanghai for Science and Technology, Shanghai 200093, China (e-mail: qbzheng@usst.edu.cn).

Zhao Wang is with the Southern University of Science and Technology, Shenzhen 518055, China, and International Quantum Academy, Shenzhen 518048, China. (Jianjun Wang and Zhao Wang contributed equally to this work.)

information of muon pulse signals by performing frequency and phase fitting analysis on their cross-correlation function. Additionally, the averaging effect inherent in the cross-correlation process minimizes measurement errors, ensuring high accuracy and resolution in time interval measurements. In this study, to validate the feasibility of the proposed method, we designed an electronic measurement prototype. This prototype utilizes an ADC operating at a rate of 40 MSPS to digitize the muon signals, and the time measurement algorithm based on phase fitting is implemented within an FPGA. A high-precision time measurement can be achieved without requiring an independent time circuit. Moreover, the low-speed ADCs not only meet the measurement requirements for time and energy information but also effectively prevent data redundancy, thereby simplifying the system. Building upon this, we assembled a muon detector array for joint cosmic ray testing to assess the applicability of the method in muon detection systems. The test results presented in this study suggest that it is possible to develop readout electronics with higher integration and lower resource consumption based on this method for application in multi-channel muon detection systems.

This paper is organized as follows: Section II introduces the principles of phase-fitting measurement. Additionally, the method is subjected to measurement error analysis and simulation validation. In Section III, a prototype is designed and implemented, followed by electronics test and cosmic ray test to assess its performance. A summary of this research and the discussion of future improvements are given in Section IV.

## II. THEORETICAL ANALYSIS

### A. Time Measurement Based on Phase-Fitting

In a typical muon detection system, muon pulse signals are

usually amplified and shaped by the front-end amplifier (FEA) after passing through the detector, resulting in a series of pulse signals with similar spectral information. After FEA processing, the procedure for the time measurement method is depicted in Fig. 1. Two muon pulse signals with a time interval  $\tau$  are digitized by the ADCs and subsequently sent to the processor for further analysis. Initially, the digitized signals are transformed into frequency domain signals through discrete Fourier transform (DFT). Then, the cross-correlation operations are applied to the signals to extract the frequency and phase information of their cross-correlation functions. Theoretical analysis indicates that a linear relationship exists between the phase and frequency, with the slope of this relationship being dependent on time interval. Consequently, time measurement is achieved through the application of a phase fitting algorithm.

The muon pulse signals  $s_1(t)$ ,  $s_2(t)$  in Figure 1 with a time interval  $\tau$  can be expressed as:

$$s_1(t) = s(t) \quad (1)$$

$$s_2(t) = s(t - \tau). \quad (2)$$

The digitized signal  $x_1(nT_s)$ ,  $x_2(nT_s)$  obtained after sampling with the ADCs can be expressed as:

$$x_1(nT_s) = s_1(nT_s) + w_1(nT_s) \quad (3)$$

$$x_2(nT_s) = s_2(nT_s) + w_2(nT_s) \quad (4)$$

where  $w_1(nT_s)$ ,  $w_2(nT_s)$  represent the noise signal introduced by the circuit. Furthermore, according to the correlation theorem [27], performing cross-correlation on the obtained digital signals and applying the DFT yields:

$$\begin{aligned} R(k) &= X_1(k)X_2^*(k) \\ &= S_1(k)S_2^*(k) + S_1(k)W_2^*(k) + S_2^*(k)W_1(k) + W_1(k)W_2^*(k). \end{aligned} \quad (5)$$

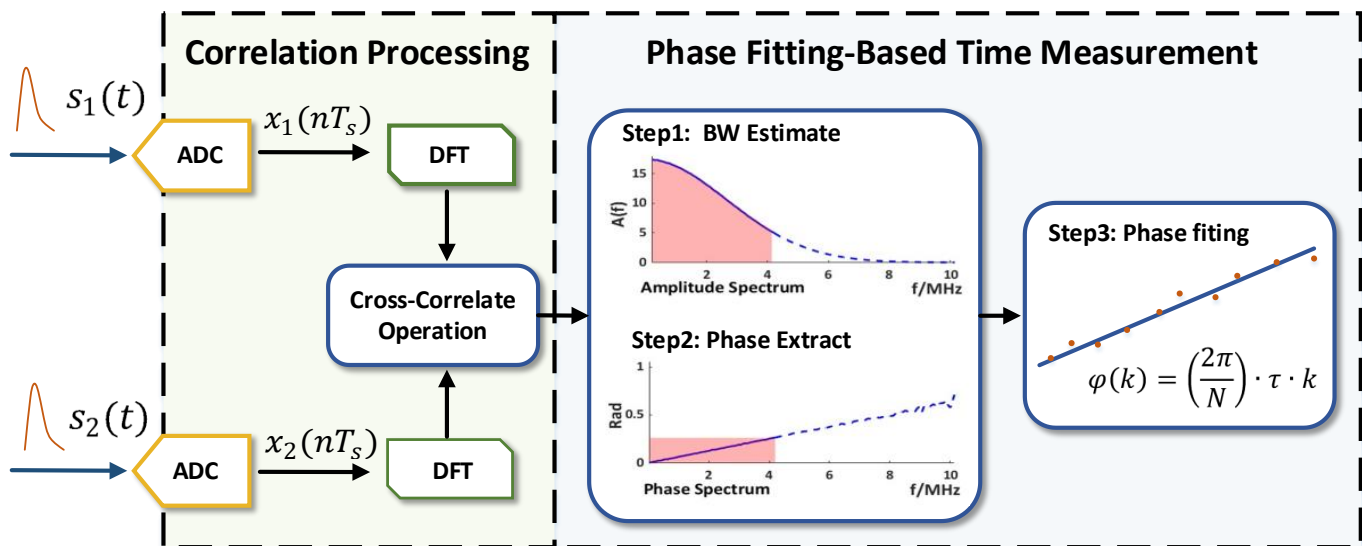


Fig. 1. Block diagram of high precision time measurement of nuclear pulse events based on the phase-fitting method. When muon events strike the detector, they are shaped into quasi-Gaussian pulses  $s_1(t)$ ,  $s_2(t)$  through analog frontend processing.  $x_1(nT_s)$  and  $x_2(nT_s)$  represent the digital signals of the muon pulses, and  $T_s$  is the sampling period of the ADCs.  $\varphi(k)$  is the phase angle of in the bandwidth and  $k$  is the frequency.

In the expression,  $X_1(k)$ ,  $X_2(k)$ ,  $S_1(k)$ ,  $S_2(k)$ ,  $W_1(k)$ ,  $W_2(k)$  represent the spectra of  $x_1(nT_s)$ ,  $x_2(nT_s)$ ,  $s_1(nT_s)$ ,  $s_2(nT_s)$ ,  $w_1(nT_s)$ ,  $w_2(nT_s)$ , here  $k$  is the frequency. The noise is mutually independent and unrelated to the pulse signal, when the number of sampling points  $N$  is sufficiently large. Then the cross-correlation can be approximately written as:

$$R(k) \approx S_1(k)S_2^*(k) = |S(k)|^2 \exp(j \frac{2\pi}{N} k\tau). \quad (6)$$

The phase of  $R(k)$  can be expressed as:

$$\varphi(k) = \frac{2\pi}{N} k\tau. \quad (7)$$

It means the phase  $\varphi(k)$  is proportional to the frequency  $k$  and the delay time  $\tau$ . If we perform the linear regression method, the delay time  $\tau$  can be estimated as the slop of the linear relationship between phase  $\varphi(k)$  and the frequency  $k$ , denote as  $\hat{\tau}$ .

### B. Error Analysis

Furthermore, the error of estimation value  $\hat{\tau}$  was analyzed. The relationship between the phase  $\varphi_n$  and frequency points  $f_n$  can be represented as:

$$\varphi_n = 2\pi f_n \tau + \phi_0 \quad (n=0,1,\dots,N-1) \quad (8)$$

where  $\phi_0$  is the initial phase, and  $N$  refers to the number of sampling points.

Let  $\bar{y}$  denote the observation vector,  $\bar{x}$  denote the vector of estimated parameters, and  $J$  indicate the corresponding Jacobian determinant. Therefore, the following relationship can be established:

$$\bar{y} = J \bar{x} \quad (9)$$

where

$$\bar{y} = \begin{bmatrix} \varphi_0 \\ \varphi_1 \\ \vdots \\ \varphi_{N-1} \end{bmatrix}, \quad J = \begin{bmatrix} 2\pi f_0 & 1 \\ 2\pi f_1 & 1 \\ \vdots & \vdots \\ 2\pi f_n & 1 \end{bmatrix}, \quad \bar{x} = \begin{bmatrix} \tau \\ \phi_0 \end{bmatrix}. \quad (10)$$

Let  $\sigma_{\varphi_n}$  represent the phase error of  $\varphi_n$ , with the error matrix  $V$  given by:

$$V = \begin{bmatrix} \sigma_{\varphi_0}^2 & & & 0 \\ & \sigma_{\varphi_1}^2 & & \\ & & \ddots & \\ 0 & & & \sigma_{\varphi_{N-1}}^2 \end{bmatrix}. \quad (11)$$

The mean square error matrix  $MSE$  for the least-squares estimates  $\hat{\tau}$  and  $\hat{\phi}_0$  can be expressed as:

$$MSE = [J^T V^{-1} J]^{-1} = \frac{1}{\sum_{n=0}^{N-1} \frac{(2\pi f_n)^2}{\sigma_{\varphi_n}^2} \cdot \sum_{n=0}^{N-1} \frac{1}{\sigma_{\varphi_n}^2} - (\sum_{n=0}^{N-1} \frac{2\pi f_n}{\sigma_{\varphi_n}^2})^2} \begin{bmatrix} \sum_{n=0}^{N-1} \frac{1}{\sigma_{\varphi_n}^2} & -\sum_{n=0}^{N-1} \frac{2\pi f_n}{\sigma_{\varphi_n}^2} \\ -\sum_{n=0}^{N-1} \frac{2\pi f_n}{\sigma_{\varphi_n}^2} & \sum_{n=0}^{N-1} \frac{(2\pi f_n)^2}{\sigma_{\varphi_n}^2} \end{bmatrix}. \quad (12)$$

In(12), as described by Takahashi et al. (2000),  $\sigma_{\varphi_n}^2$  can be approximated as a constant value  $\sigma_{\varphi}^2$  which is inversely proportional to the signal-to-noise ratio at the corresponding frequency point of the cross-correlation function ( $SNR_n$ ) [28]:

$$\sigma_{\varphi}^2 = \frac{A}{SNR_n} \quad (13)$$

where  $A$  is the coefficient. The  $SNR_n$  is found by dividing the  $SNR$  of the output signal from cross-correlation function ( $SNR_o$ ) into  $N$  parts [28]:

$$SNR_o = N \cdot SNR_n. \quad (14)$$

Then the  $MSE$  can be represented as:

$$MSE = \frac{\sigma_{\varphi}^2}{4\pi^2 N^2 \left\{ \frac{1}{N} \sum_{n=0}^{N-1} f_n^2 - \left( \frac{1}{N} \sum_{n=0}^{N-1} f_n \right)^2 \right\}} \begin{bmatrix} N & -2\pi \sum_{n=0}^{N-1} f_n \\ -2\pi \sum_{n=0}^{N-1} f_n & 4\pi^2 \sum_{n=0}^{N-1} f_n^2 \end{bmatrix} \approx \frac{A}{4\pi^2 N \cdot SNR_o \cdot \left\{ \frac{1}{N} \sum_{n=0}^{N-1} f_n^2 - \left( \frac{1}{N} \sum_{n=0}^{N-1} f_n \right)^2 \right\}} \begin{bmatrix} N & -2\pi \sum_{n=0}^{N-1} f_n \\ -2\pi \sum_{n=0}^{N-1} f_n & 4\pi^2 \sum_{n=0}^{N-1} f_n^2 \end{bmatrix} \quad (15)$$

where  $\frac{1}{N} \sum_{n=0}^{N-1} f_n$  can be represented as the sample mean of the frequency  $\bar{f}$ . The sample variance of the frequency  $\sigma_f^2$  is given by:

$$\sigma_f^2 = \frac{1}{N} \sum_{n=0}^{N-1} (f_n - \bar{f})^2 = \frac{1}{N} \sum_{n=0}^{N-1} f_n^2 - \left( \frac{1}{N} \sum_{n=0}^{N-1} f_n \right)^2. \quad (16)$$

Substituting (16) into (15), the  $MSE$  can be expressed as:

$$MSE = \frac{A}{4\pi^2 SNR_o \cdot \sigma_f^2} \begin{bmatrix} 1 & -2\pi \bar{f} \\ -2\pi \bar{f} & 4\pi^2 \bar{f}^2 \end{bmatrix}. \quad (17)$$

The error  $\varepsilon$  associated with the estimate  $\hat{\tau}$  is expressed as:

$$\varepsilon = \hat{\tau} - \tau = \left( \frac{A}{4\pi^2 \cdot SNR_o \cdot \sigma_f^2} \right)^{\frac{1}{2}}. \quad (18)$$

Furthermore, for bandpass signals,  $\sigma_f^2$  can be approximated as:

$$\sigma_f^2 \approx \frac{1}{f_B} \int_0^{f_B} \left(f - \frac{f_B}{2}\right)^2 df = \frac{f_B^2}{12} \quad (19)$$

where  $f_B$  represents the signal bandwidth. Substituting (19) into (18) yields:

$$\varepsilon \approx \frac{\sqrt{3 \cdot A}}{\pi \cdot f_B \cdot \sqrt{SNR_o}}. \quad (20)$$

Given the characteristics of the muon detector, the  $f_B$  is determined. Consequently, it can be inferred from (20) that  $\varepsilon$  decreases as the  $SNR_o$  increases, thereby leading to improved measurement precision. In general, as the SNR of the input signal increases, the  $SNR_o$  also improves accordingly [29].

### C. Simulation

In order to validate this method, a simulation model is developed on the MATLAB platform. As shown in Fig. 2, the Gaussian pulse signals with noise and the ideal Gaussian pulse signals are used as test signals for theoretical calculations and simulation verification. By subtracting the cross-correlation output signal power  $P_1$  of the ideal signals from the cross-correlation output signal power  $P_2$  of the signals with noise, the noise power is obtained. Subsequently, the  $SNR_o$  is calculated under the noise conditions, and this value is substituted into (20) to determine the theoretical precision. Additionally, the standard deviation (STD) of the estimated time results is calculated through Monte Carlo simulations.

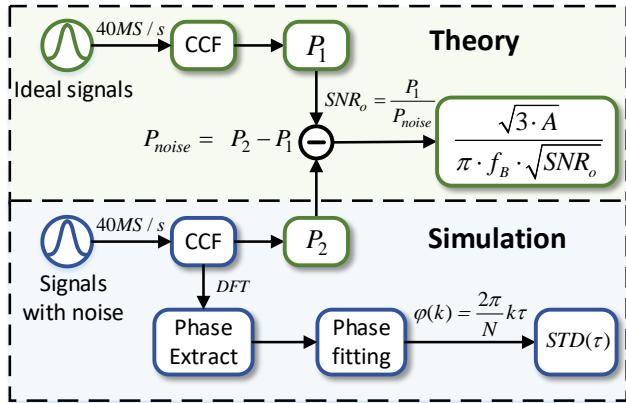


Fig. 2. The process of the theoretical calculation and simulation.  $P_1$  refers to the output power of the cross-correlation function (CCF) for the ideal pulse signals.  $P_2$  refers to the output power of the CCF for signals with noise. The noise power  $P_{noise}$  is obtained by subtracting  $P_1$  from  $P_2$ . Then, the  $SNR_o$  can be calculated and used to determine the theoretical precision.

The detector response of the muon event was simulated as a Gaussian pulse signal with certain parameters. In this paper below, we use the pulse width of 200ns with the frequency band width  $f_B$  of 7.92MHz, the SNR of the Gaussian signal is 100dB. These pulses are sampled at a rate of 40 MSPS, a set of 512 samples was collected in one simulating turn. By comparing the signal power of the cross-correlation function of these input pulses with that of ideal Gaussian pulses, the  $SNR_o$  is calculated to be 111.35 dB. The theoretical Standard

Deviation (STD) calculated using (20) is  $0.196\sqrt{A}$  ps RMS. Additionally, the STD is found to be 0.52 ps RMS following 10,000 statistical results from Monte Carlo simulations under the same input conditions. Therefore, the coefficient A is different from various experiments, without the loss of the generality, The value A can be approximated as 7.00 in this paper. Then, we have introduced more Gaussian white noise into the input signals to further analyze the impact of  $SNR$  on time precision. Theoretical calculations and simulation are performed for input signals with SNR conditions ranging from 30 dB to 100 dB. Meanwhile, the consistency between Monte Carlo simulation results and theoretical precision was observed at sampling rates of 20 MSPS, 40 MSPS, and 80 MSPS. The results are presented in Fig. 3, indicating that this method can achieve high precision in time measurement under conditions of high  $SNR$ .

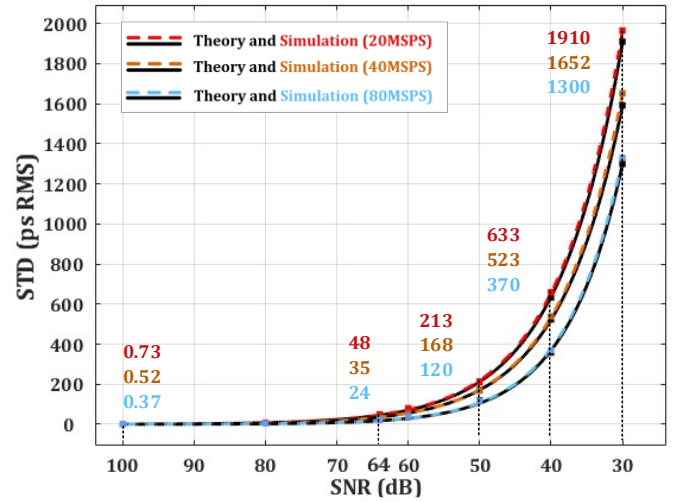


Fig. 3. The trend of the theoretical precision and the Monte Carlo simulation precision under SNR ranging from 30 dB to 100 dB, with sampling rates of 20 MSPS, 40 MSPS, and 80 MSPS.

## III. EXPERIMENTS AND RESULTS

To validate the feasibility of the method proposed in this paper, a phase-fitting time measurement module (PF-TMM) is developed. Following this, an experimental platform is assembled, which primarily includes the PF-TMM, a signal source, and a muon detector to evaluate its time performance.

### A. Introduction to PF-TMM

The block diagram of the design of PF-TMM is shown in Fig. 3. It employs the ADS5263 as the ADC chip to achieve a 40 MSPS sampling rate and 16-bit resolution for muon pulse signal sampling. Additionally, an FPGA serves as its digital processor, facilitating time measurement based on phase-fitting and system configuration. The FPGA provides robust parallel processing capabilities and high flexibility, enabling real-time data acquisition and rapid signal processing. Therefore, the PF-TMM operates independently of high-frequency sampling clocks and complex circuits, effectively reducing power consumption and costs. Table 1 presents the resource evaluation results for implementing this method on the FPGA within the

prototype, which utilizes the Xilinx Kintex-7 series chip, specifically the xc7k325tffg900-2 model.

In digital logic, A pulse trigger module is implemented to improve the effective pulse event rate. Upon receiving data from the trigger module, the phase fitting module executes a phase-fitting algorithm based on cross correlation to estimate TOF information. The acquired time information is output to the host computer for further analysis.

TABLE I

RESOURCE EVALUATION OF PHASE FITTING METHOD IMPLEMENTATION IN FPGA

FPGA resources	Occupied	Available	Utilization
Occupied Slices	5762	50950	11%
Slice Luts	16702	203800	8%
Slice Flip-Flops	20888	407600	5%
BRAM	31	445	7%
Bonded IOBs	78	500	16%
DSPs	52	840	6%

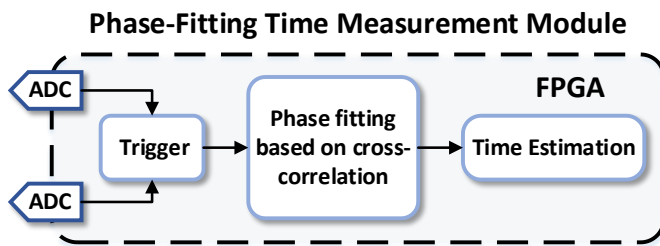


Fig. 3. The main design of phase-fitting time measurement module.

### B. Performance of the Method

A testing platform was set up in the laboratory using the Tektronix AFG31000 arbitrary waveform generator. Gaussian pulses were generated to simulate muon signals from the muon detector and were input into the PF-TMM for performance evaluation of the method. The test conditions were as follows: the Gaussian pulse width was set to 200 ns, the TOF between channels was 10 ns, the sampling clock rate was 40 MSPS, and 512 data points were sampled after exceeding the threshold for time measurement based on phase fitting.

The acquired digital signals were processed offline on a host computer for signal and noise power analysis. The best achievable SNR for the input signals on this platform was 64 dB. Under these conditions, the statistical results of 10000-time measurements between channels are shown in Fig. 4(a). The average measured time interval is 10.07 ns, with the STD of the Gaussian fit curve being 44.6 ps RMS. The prototype can achieve optimal time precision better than 50 ps.

Further analysis was performed by adding controlled noise to the test pulses. The time precision of the method at varying input signal SNRs, ranging from 30 dB to 60 dB, was compared with the theoretical precision, as shown in Fig. 3. As shown in Fig. 4(b), when the input signal SNR exceeds 40 dB, the method achieves time measurement precision almost 600ps. When the SNR further decreases to 30 dB, the method achieves a time precision of 1.75 ns. The theoretical value is slightly better than the measured precision, possibly due to FPGA resource constraints.

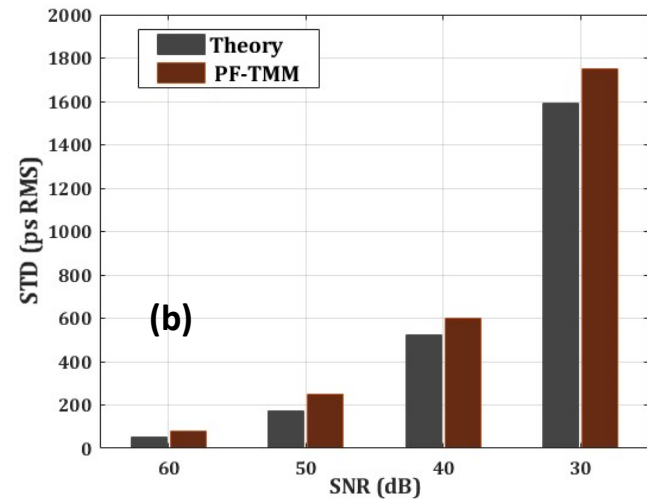
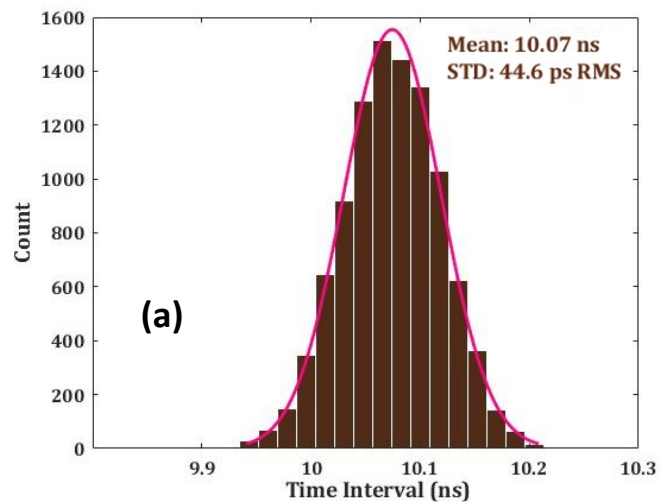


Fig. 4. (a) The typical test histogram of the measured time intervals under an SNR of 64 dB. (b) The STD comparison between the theory and PF-TMM under the SNR ranging from 30 dB to 60 dB.

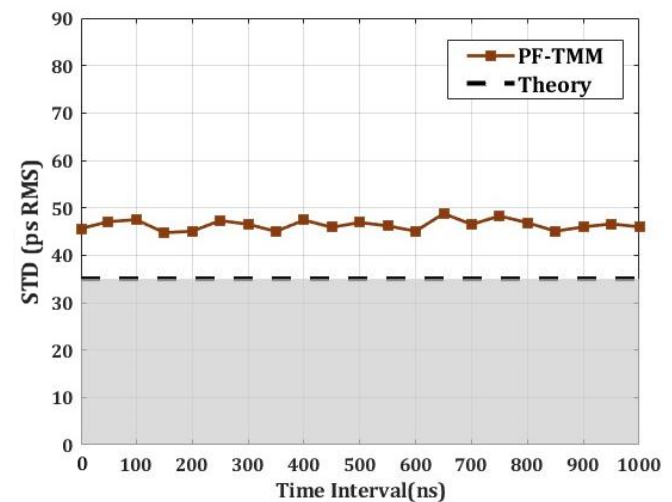


Fig. 5. Comparison of the test STD of PF-TMM with the theoretical STD under the same SNR of 64 dB, with time intervals ranging from 0 ns to 1  $\mu$ s. The dynamic range of the STD measured by PF-TMM is 40ps RMS–50 ps RMS. The theoretical STD is 35 ps RMS.

Finally, the time precision across a dynamic range of time



interval from 0 ns to 1  $\mu$ s is presented in Fig. 5. The results show that, under a 64 dB SNR condition, the method maintains an STD between 40 ps RMS and 50 ps RMS across the time interval range from 0 ns to 1  $\mu$ s, demonstrating the reliability and stability of the method implemented by the PF-TMM.

### C. Cosmic Ray Test

The block diagram of the cosmic ray test with the detector is shown in Fig. 6. The structure of the muon detector channel is based on a scintillator detector with SiPM, comprising four key components: plastic scintillator, fibers, SiPM, and charge sensitive amplifier (CSA) for channel readout [30]. In this study, the scintillator bars were manufactured by GAONENKEDI company[31] using polyethylene extrusion technology [32], while the SiPM is the S13360 series of MPPCs (with a pixel size of 50  $\mu$ m, produced by Hamamatsu). In addition, the fibers were sourced from Kuraray [33].

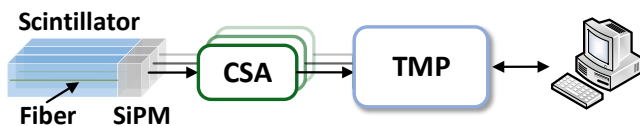


Fig. 6. The block diagram of cosmic ray test. The scintillator, fiber, and SiPM constitute the scintillator detector with SiPM. The cosmic ray signals are amplified and shaped by the charge sensitive amplifier (CSA).

The platform of the cosmic ray test is shown in Fig. 7. When the operating voltage for the detectors was set to the optimal value of 36 V. The cosmic ray signals observed after amplification through the CSA are shown in Fig. 8(a), with a signal pulse width of approximately 200 ns. Given that cosmic rays propagate at nearly the speed of light, the signals respond almost simultaneously, and the time intervals between signals from different channels can be approximated as 0 ns.

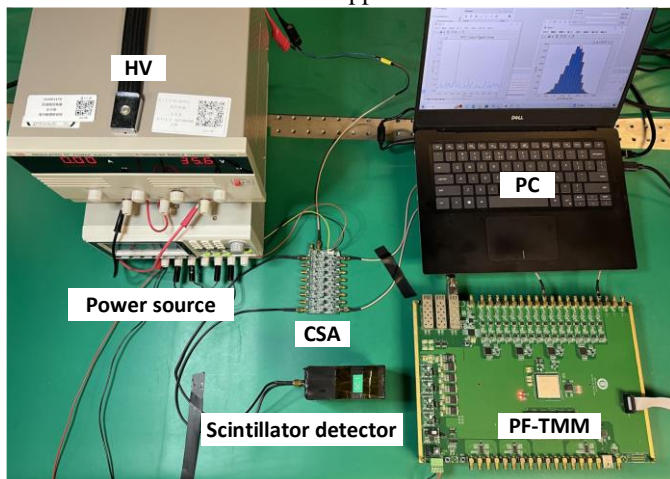


Fig. 7. The test platform for cosmic rays, including the SiPM detector, preamplifiers, electronics prototype, power supply, and display device.

During the testing, given the relatively low occurrence rate of cosmic-ray muons within the coverage area, it was necessary to collect as many muon events as possible to minimize statistical errors. Following continuous testing exceeding 24 hours, more than 1000 valid muon events were collected. The histogram of the data is presented in Fig. 8(b), the average measured channel time interval is 882 ps with the STD of the

single channel being 4.63 ns RMS. Independent testing and analysis of this detector front-end indicate that the time resolution of the detector channels is approximately 4.3 ns RMS [34], with the output muon pulses SNR of approximately 30 dB. The results demonstrate that, under the conditions, the proposed method prototype contributes 1.7 ns RMS to the cosmic ray time precision which coincides with the theoretical results in Fig. 3 of the previous section.

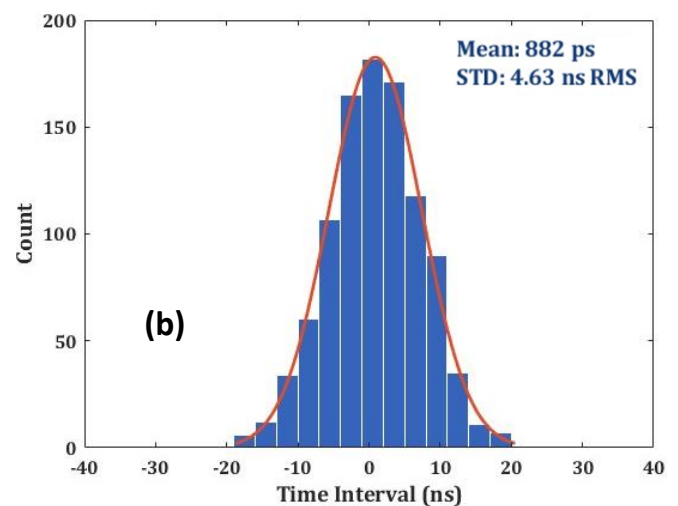
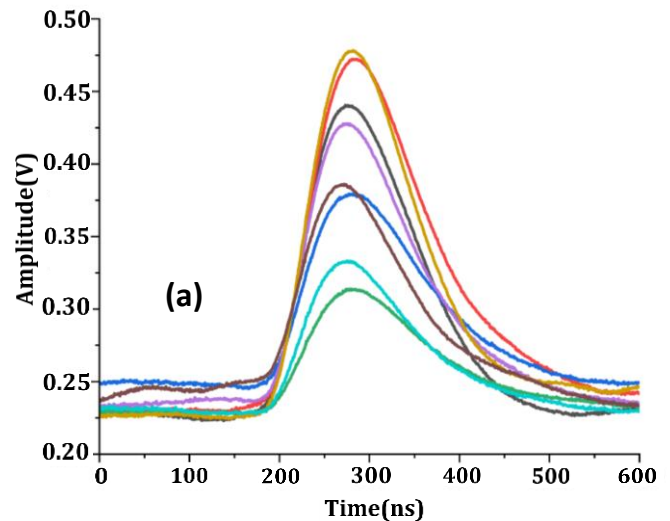


Fig. 8. (a) the oscilloscope-captured waveforms of cosmic rays. (b) the test histogram of time interval in cosmic ray testing.

## IV. CONCLUSION

This paper presents a high-precision time measurement method intended for muon detection systems. The method effectively utilizes the time information within the ADCs digital waveforms which were originally intended for energy measurement, by applying cross-correlation and phase-fitting techniques. Based on theoretical analysis, the PF-TMM was designed and fabricated. It digitizes the muon pulse signals based on phase fitting within the FPGA. This method does not rely on high-frequency sampling clocks or the independent time circuit, effectively simplifying the system, reducing power

consumption, and lowering cost. The test results indicate that, using a 40 MSPS sampling rate on the input pulse signals with a 64 dB SNR, the prototype can achieve optimal time precision better than 50 ps. And the results of cosmic ray testing validate the feasibility of the electronic prototype in muon detection. Theoretical analysis and experimental results demonstrate that this method is a reliable and practical solution for high-precision time measurement, offering a viable approach for muon detection. And it is also applicable to the measurement of other nuclear pulses.

#### ACKNOWLEDGMENT

The authors would like to thank Xiaolong Wang and Xiyang Wang at Key Laboratory of Nuclear Physics and Ion-beam Application, Fudan University for useful discussions.

#### REFERENCES

- [1] S. H. Neddermeyer and C. D. Anderson, "Note on the Nature of Cosmic-Ray Particles," *Physical Review*, vol. 51, no. 10, pp. 884-886, 05/15/ 1937, doi: 10.1103/PhysRev.51.884.
- [2] G. Particle Data *et al.*, "Review of Particle Physics," *Physical Review D*, vol. 98, no. 3, p. 030001, 08/17/ 2018, doi: 10.1103/PhysRevD.98.030001.
- [3] S. Müller, R. Engel, T. Pierog, and M. Roth, "Impact of muon detection thresholds on the separability of primary cosmic rays," *Astroparticle Physics*, vol. 97, pp. 174-185, 2018/01/01/ 2018, doi: <https://doi.org/10.1016/j.astropartphys.2017.11.005>.
- [4] N. O. Collaboration *et al.*, "Seasonal variation of multiple-muon cosmic ray air showers observed in the NOvA detector on the surface," *Physical Review D*, vol. 104, no. 1, p. 012014, 07/30/ 2021, doi: 10.1103/PhysRevD.104.012014.
- [5] K. Morishima *et al.*, "Discovery of a big void in Khufu's Pyramid by observation of cosmic-ray muons," *Nature*, vol. 552, no. 7685, pp. 386-390, 2017/12/01 2017, doi: 10.1038/nature24647.
- [6] V. M. Bondarenko, V. I. Brovkin, A. G. Tarkhov, V. Y. Chertkov, V. N. Polyakov, and L. B. Prozorov, "Application of the muon method to the determination of the density of rocks in the case of a background of high radioactivity," *Soviet Atomic Energy*, vol. 36, no. 6, pp. 656-658, 1974/06/01 1974, doi: 10.1007/BF01127243.
- [7] T. C. S. Group, "CEPC Conceptual Design Report: Volume 1 - Accelerator," 2018.
- [8] T. Group, *CEPC Conceptual Design Report: Volume 2 - Physics & Detector*. 2018.
- [9] P. D. Group *et al.*, "Review of Particle Physics," *Progress of Theoretical and Experimental Physics*, vol. 2022, no. 8, 2022, doi: 10.1093/ptep/ptac097.
- [10] T. Hebbeker and K. Hoepfner, "Muon Spectrometers," in *Handbook of Particle Detection and Imaging*, I. Fleck, M. Titov, C. Grupen, and I. Buvat Eds. Cham: Springer International Publishing, 2020, pp. 1-26.
- [11] Y. Wang *et al.*, "A High Spatial Resolution Muon Tomography Prototype System Based on Micromegas Detector," *IEEE Transactions on Nuclear Science*, vol. 69, no. 1, pp. 78-85, 2022, doi: 10.1109/TNS.2021.3137415.
- [12] J. Pan *et al.*, "Position Encoding Readout Electronics of Large Area Micromegas Detectors aiming for Cosmic Ray Muon Imaging," in *2019 IEEE Nuclear Science Symposium and Medical Imaging Conference (NSS/MIC)*, 26 Oct.-2 Nov. 2019 2019, pp. 1-5, doi: 10.1109/NSS/MIC42101.2019.9060024.
- [13] W. Liu, T. Wei, B. Li, P. Guo, and Y. Hu, "Design of a 12-bit 1MS/s SAR-ADC for front-end readout of 32-channel CZT detector imaging system," *Nuclear Instruments and Methods in Physics Research Section A: Accelerators, Spectrometers, Detectors and Associated Equipment*, vol. 786, pp. 155-163, 2015/06/21/ 2015, doi: <https://doi.org/10.1016/j.nima.2015.03.049>.
- [14] Y. Sun *et al.*, "The prototype of the front-end electronics for STCF muon detector," *Nuclear Instruments and Methods in Physics Research Section A: Accelerators, Spectrometers, Detectors and Associated Equipment*, vol. 1065, p. 169528, 2024/08/01/ 2024, doi: <https://doi.org/10.1016/j.nima.2024.169528>.
- [15] S. Xiang, F. Dou, and H. Liang, "The readout electronics for the drift chamber based cosmic ray muon radiography of high-Z materials," in *2014 19th IEEE-NPSS Real Time Conference*, 26-30 May 2014 2014, pp. 1-6, doi: 10.1109/RTC.2014.7097518.
- [16] S.-T. Xiang and H. Liang, "A time and charge measurement board for muon tomography of high-Z materials," *Nuclear Science and Techniques*, vol. 28, no. 3, p. 40, 2017/02/17 2017, doi: 10.1007/s41365-017-0183-1.
- [17] Y. Zoccarato *et al.*, "Front end electronics and first results of the ALICE V0 detector," *Nuclear Instruments and Methods in Physics Research Section A: Accelerators, Spectrometers, Detectors and Associated Equipment*, vol. 626-627, pp. 90-96, 2011/01/11/ 2011, doi: <https://doi.org/10.1016/j.nima.2010.10.025>.
- [18] H. Hernández *et al.*, "A Monolithic 32-Channel Front End and DSP ASIC for Gaseous Detectors," *IEEE Transactions on Instrumentation and Measurement*, vol. 69, no. 6, pp. 2686-2697, 2020, doi: 10.1109/TIM.2019.2931016.
- [19] F. Li *et al.*, "Performance of Pad Front-End Board for Small-Strip Thin Gap Chamber With Cosmic Ray Muons," *IEEE Transactions on Nuclear Science*, vol. 65, no. 1, pp. 597-603, 2018, doi: 10.1109/TNS.2017.2775229.
- [20] M. D. Matteis *et al.*, "An Eight-Channels 0.13-  $\mu\text{m}$  - CMOS Front End for ATLAS Muon-Drift-Tubes Detectors," *IEEE Sensors Journal*, vol. 17, no. 11, pp. 3406-3415, 2017, doi: 10.1109/JSEN.2017.2694606.
- [21] Y. Sato *et al.*, "Performance of Front-end ASIC and its evaluation with Silicon Strip Sensor for J-PARC Muon g-2/EDM Experiment," in *2017 IEEE Nuclear Science Symposium and Medical Imaging Conference (NSS/MIC)*, 21-28 Oct. 2017 2017, pp. 1-3, doi: 10.1109/NSSMIC.2017.8532754.
- [22] Y. Arai and T. Emura, "Development of a 24 ch TDC LSI for the ATLAS Muon Detector," 2000.
- [23] P. Bifulco *et al.*, "A fully-digital and fully synthesizable TDC for high energy physics experiments," in *2016 Second International Conference on Event-based Control, Communication, and Signal Processing (EBCCSP)*, 13-15 June 2016 2016, pp. 1-4, doi: 10.1109/EBCCSP.2016.7605283.
- [24] J. Wang, C. Feng, W. Dong, Z. Shen, and S. Liu, "A High Precision Time-to-Digital Converter based on Multi-chain Interpolation with a Low Cost Artix-7 FPGA," in *2021 7th International Conference on Event-Based Control, Communication, and Signal Processing (EBCCSP)*, 22-25 June 2021 2021, pp. 1-5, doi: 10.1109/EBCCSP53293.2021.9502368.
- [25] P. Carra *et al.*, "Auto-Calibrating TDC for a SoC-FPGA Data Acquisition System," in *2017 IEEE Nuclear Science Symposium and Medical Imaging Conference (NSS/MIC)*, 21-28 Oct. 2017 2017, pp. 1-2, doi: 10.1109/NSSMIC.2017.8533060.
- [26] N. Roy *et al.*, "Low Power and Small Area, 6.9 ps RMS Time-to-Digital Converter for 3-D Digital SiPM," vol. 1, pp. 486-494, 2017.
- [27] E. C. Ifeachor, B. W. Jervis, E. L. Dagless, and J. O'Reilly, "Digital Signal Processing: A Practical Approach," 1993.
- [28] I. F. Takahashi, T. Kondo, Y. Takahashi, Y. J. I. A. Koyama, and E. S. Magazine, "Very long baseline interferometer," vol. 17, pp. 43-44, 2002.
- [29] Z. Xue, J. Charonko, and P. Vlachos, "Particle image velocimetry correlation signal-to-noise ratio metrics and measurement uncertainty quantification," *Measurement Science and Technology*, vol. 25, 09/22 2014, doi: 10.1088/0957-0233/25/11/115301.
- [30] X.-Y. Wang *et al.*, "Design and performance of a high-speed and low-noise preamplifier for SiPM," *Nuclear Science and Techniques*, vol. 34, no. 11, p. 169, 2023/11/18 2023, doi: 10.1007/s41365-023-01328-7.
- [31] B. G. K. T. C. L. (China). <http://www.gaonengkeji.com/> (accessed 12 Nov., 2024).
- [32] A. Pla-Dalmau, A. D. Bross, and K. L. Mellott, "Low-cost extruded plastic scintillator," *Nuclear Instruments and Methods in Physics Research Section A: Accelerators, Spectrometers, Detectors and Associated Equipment*, vol. 466, no. 3, pp. 482-491, 2001/07/11/ 2001, doi: [https://doi.org/10.1016/S0168-9002\(01\)00177-2](https://doi.org/10.1016/S0168-9002(01)00177-2).
- [33] L. J. Kuraray. <https://www.kuraray.com/products/psf> (accessed 12 Nov, 2024).

- [34] CAEN. "User Manual UM4270: DT5742—16+1 Channel 12bit 5 GS/s Switched Capacitor Digitizer URL." <https://www.caen.it/products/dt5742/> (accessed 12 Nov, 2024).